10.24425/acs.2020.134678

Archives of Control Sciences
Volume 30(LXVI), 2020
No. 3, *pages* 575–597

A new 4-D hyperchaotic system with no equilibrium, its multistability, offset boosting and circuit simulation

SUNDARAPANDIAN VAIDYANATHAN, IRENE M. MOROZ and ACENG SAMBAS

A new 4-D dynamical system with hyperchaos is reported in this work. It is shown that the proposed nonlinear dynamical system with hyperchaos has no equilibrium point. Hence, the new dynamical system exhibits hidden hyperchaotic attractor. An in-depth dynamic analysis of the new hyperchaotic system is carried out with bifurcation transition diagrams, multistability analysis, period-doubling bubbles and offset boosting analysis. Using Integral Sliding Mode Control (ISMC), global hyperchaos synchronization results of the new hyperchaotic system are described in detail. Furthermore, an electronic circuit realization of the new hyperchaotic system has been simulated in MultiSim software version 13.0 and the results of which are in good agreement with the numerical simulations using MATLAB.

Key words: chaos, chaotic systems, hidden attractors, sliding mode control, circuit design, synchronization

1. Introduction

Hyperchaotic systems are nonlinear dynamical systems with more complex solutions than chaotic dynamical systems. Hyperchaotic systems are characterized by the presence of more than one positive Lyapunov exponent (LE). For a 4-D autonomous hyperchaotic system, there are two positive Lyapunov exponents, one zero and one negative Lyapunov exponent [1]. Hyperchaotic systems are applied in several engineering areas such as lasers [2, 3], power systems [4, 5], oscillators [6–10], neural networks [11–14], cryptosystems [15–18], neurons [19, 20], memristors [21–23], etc.

S. Vaidyanathan (corresponding Author) E-mail: sundarvtu@gmail.com, is with DSchool of Electrical and Computing, Vel Tech University, 400 Feet Outer Ring Road, Avadi, Chennai-600092, Tamil Nadu, India.

I.M. Moroz, E-mail: Irene.Moroz@maths.ox.ac.uk, is with Mathematical Institute, University of Oxford, Andrew Wiles Building, ROQ, Oxford Ox2 6GG, UK.

A. Sambas, E-mail: acengs@umtas.ac.id, is with Department of Mechanical Engineering, Universitas Muhammadiyah Tasikmalaya, Tasikmalaya 46196, West Java, Indonesia.

Received 2.12.2019.

Chaotic dynamical systems have been recently classified into two categories *viz.* systems with self-excited and hidden attractors [24]. A chaotic attractor is called self-excited if its basin of attraction involves at least one equilibrium. Otherwise, the chaotic attractor is called a hidden attractor. Chaotic and hyperchaotic systems with no equilibrium [25,26] or stable equilibrium points [27,28] possess hidden attractors [1]. In recent years, modelling and control of hidden attractors have received great interest in the literature [29–32].

In this work, we report a new hyperchaotic dynamical system with no equilibrium. Thus, the new dynamical system exhibits hidden hyperchaotic attractor [1]. An in-depth dynamic analysis of the new hyperchaotic system is carried out with Lyapunov exponents and bifurcation transition diagrams.

Multistability signifies the coexistence of attractors in a dynamical system for the same parameter values [33]. In recent years, there is great research on chaotic and hyperchaotic systems with multistability in the literature [34–36]. In this work, we show that the new hyperchaotic system exhibits multistability with three coexisting attractors for three different initial conditions. Offset boosting of chaotic attractors has received good interest in the literature [37, 38]. In this work, we also discuss the offset boosting of the new hyperchaotic system.

As a control application, new results are derived for the global hyperchaos synchronization of the new hyperchaotic system with itself using Integral Sliding Mode Control (ISMC). There are many methods for control and synchronization of systems such as active control [39, 40], adaptive control [41–43], etc. The sliding mode control method is an useful method in control applications, as it has attractive features such as fast convergence, disturbance rejection and robustness [44, 45].

Circuit realization of chaotic and hyperchaotic systems is very useful for their practical implementation [46–49]. In this work, an electronic circuit realization of the new hyperchaotic system has been simulated in MultiSim software version 13.0 and the results of which are in good agreement with the numerical simulations using MATLAB.

2. A new 4-D hyperchaotic system with no equilibrium

2.1. System dynamics and properties

In this research work, we consider a new 4-D dynamical system given by

$$\begin{cases} \dot{x} = a(y-x), \\ \dot{y} = 2x(1-z) + cy + w, \\ \dot{z} = xy - b, \\ \dot{w} = -d(x+y) \end{cases} \tag{1}$$

with states x, y, z, w and real constants a, b, c, d. It is noted that the new system (1) has a total of ten terms on the right hand side with only two quadratic nonlinear terms, *viz.* xy and xz.

To simplify the notation, we denote $X = (x, y, z, w)$ to represent the state of the system (1).

In this work, we show that the system (1) is *hyperchaotic* when the system parameters assume the values

$$a = 31, \quad b = 25, \quad c = 15, \quad d = 3.3. \tag{2}$$

Using Wolf's algorithm [50], the Lyapunov exponents of the new system (1) are numerically estimated for the parameter values $(a, b, c, d) = (31, 25, 15, 3.3)$ and initial state $X(0) = (0.2, 0.1, 0.2, 0.1)$ for $T = 1E6$ seconds as follows:

$$\psi_1 = 1.772, \quad \psi_2 = 0.1092, \quad \psi_3 = 0, \quad \psi_4 = -17.2834. \tag{3}$$

Since there are two positive Lyapunov exponents ψ_1 and ψ_2, the system (1) is hyperchaotic. Since the sum of the Lyapunov exponents is negative for the chosen parameter values and $X(0)$, it follows that the new hyperchaotic system (1) is dissipative. The Kaplan-Yorke dimension of the new hyperchaotic system (1) is determined as

$$D_{KY} = 3 + \frac{\psi_1 + \psi_2 + \psi_3}{|\psi_4|} = 3.0744. \tag{4}$$

The value of D_{KY} gives a measure of the high complexity of the new hyperchaotic system (1).

To determine the equilibrium points or rest points of the new system (1), we solve the following system of equations:

$$a(y - x) = 0, \tag{5a}$$

$$2x(1 - z) + cy + w = 0, \tag{5b}$$

$$xy - b = 0, \tag{5c}$$

$$-d(x + y) = 0. \tag{5d}$$

We solve the equations (5) assuming that a, b, c, d are non-zero parameters.

Since $a \neq 0$ and $d \neq 0$, the equations (5a) and (5d) yield $x = y$ and $x = -y$.

This can happen simultaneously only when $x = y = 0$. Substituting $x = y = 0$ in (5c), we get $b = 0$, which is a contradiction.

Hence, there is no solution to the system of equations (5). In other words, the new 4-D hyperchaotic system (1) has no equilibrium. Hence, it follows that the new 4-D hyperchaotic system (1) has hidden attractor. Thus, (1) is a special hyperchaotic system.

Figure 1 shows the MATLAB simulations of the phase plots of the new 4-D hyperchaotic system (1) for $(a, b, c, d) = (31, 25, 15, 3.3)$ and $X(0) = (0.2, 0.1, 0.2, 0.1)$.

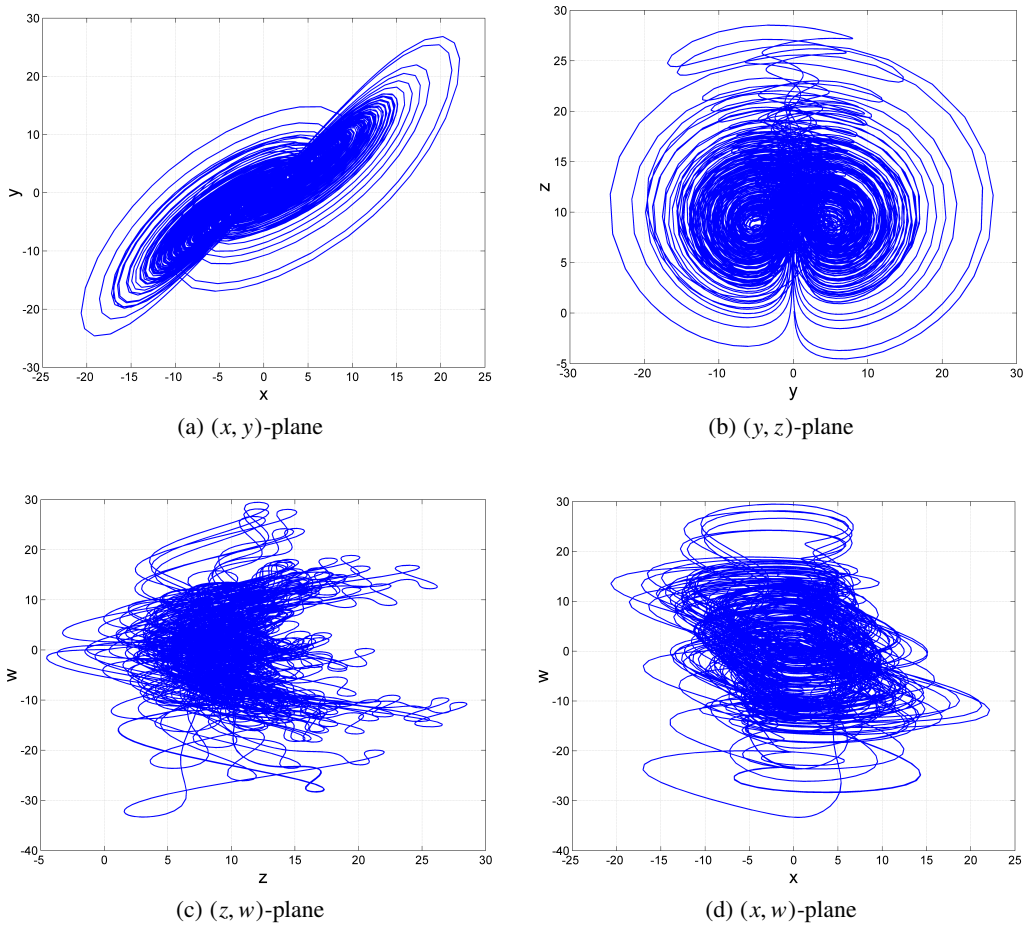

(a) (x, y)-plane (b) (y, z)-plane

(c) (z, w)-plane (d) (x, w)-plane

Figure 1: The phase portraits of the new hyperchaotic system (1) in MATLAB for $(a, b, c, d) = (31, 25, 15, 3.3)$ and $X(0) = (0.2, 0.1, 0.2, 0.1)$

2.2. Bifurcation transition diagrams

We now present the bifurcation transition diagrams as each parameter varies in turn. We show these diagrams as two-panel plots in which the parameter increases in the upper panel and decreases in the lower panel. This enables us to spot multiple states, caused by hysteresis. It is of interest to note that the divergence of the flow of the 4-D hyperchaotic system (1) is

$$\nabla(\dot{x}, \dot{y}, \dot{z}, \dot{w}) = c - a.$$

Therefore volumes contract in phase space provided $c < a$. For the chosen set of parameter values, *viz.* $(a, b, c, d) = (31, 25, 15, 3.3)$, this is indeed the case. This constraint is apparent in the bifurcation transition plots as the parameter a

approaches 16, by an up-turn in the maxima of $y_{\max}$ (see Figure 2). Figures 3 and 4 show sections of this bifurcation transition diagram in order to highlight the presence of hysteresis, and also multiple attractor states, which will be discussed in more detail in the next subsection.

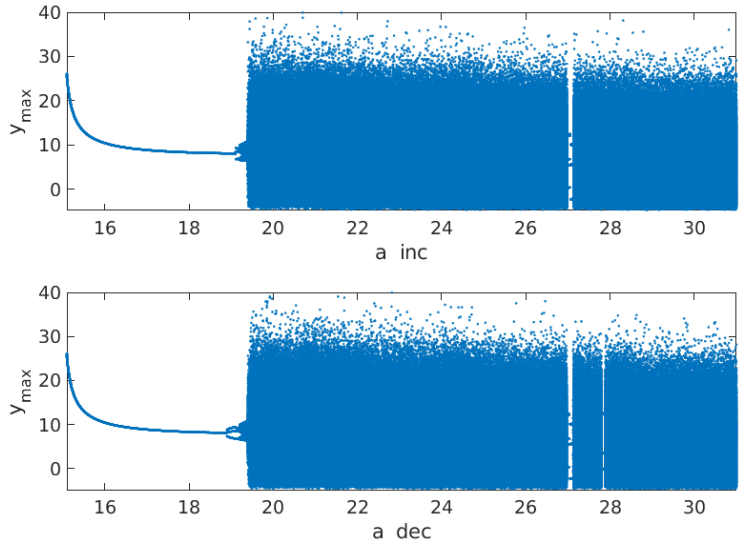

Figure 2: Bifurcation transition plots of $y_{\max}$ as a varies in $16 < a < 35$. The upper panel is for a increasing, while the lower panel is for a decreasing.

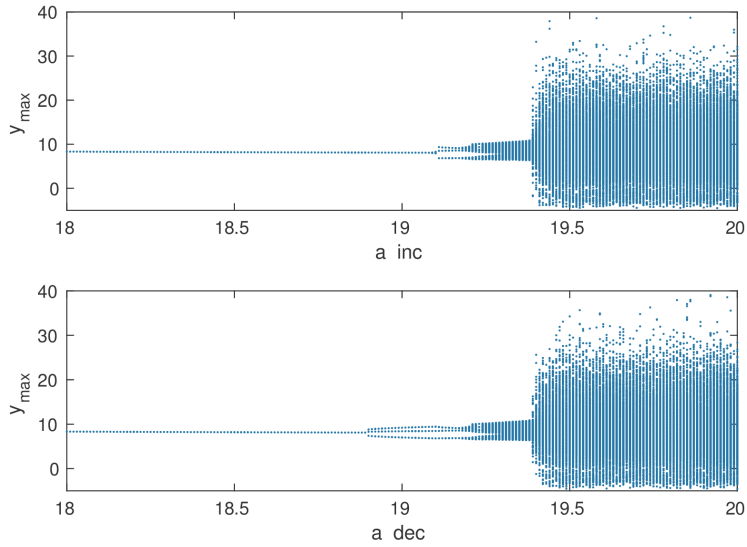

Figure 3: Bifurcation transition plots of $y_{\max}$ as a varies in $18 < a < 20$. The upper panel is for a increasing, while the lower panel is for a decreasing.

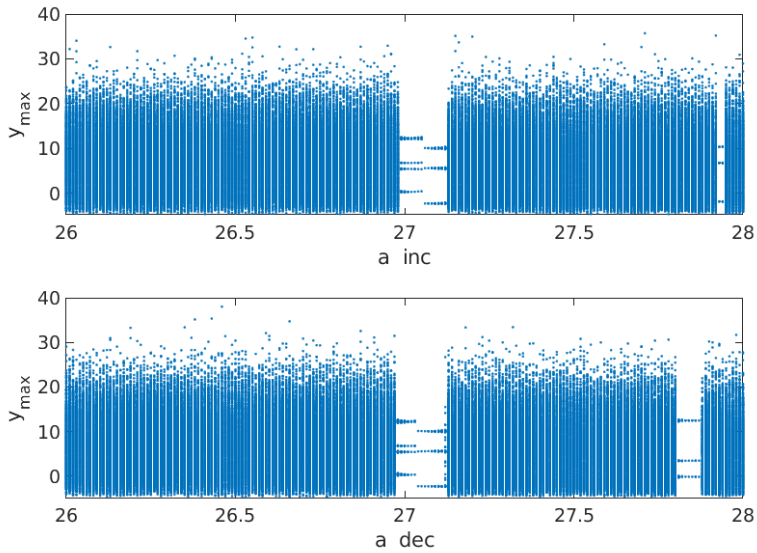

Figure 4: Bifurcation transition plots of y_{max} as a varies in $26 < a < 28$. The upper panel is for a increasing, while the lower panel is for a decreasing.

We now vary parameter b. Figure 5 shows the corresponding bifurcation plots for $0 < b < 8$. Again, there are slight differences between the upper and lower panels.

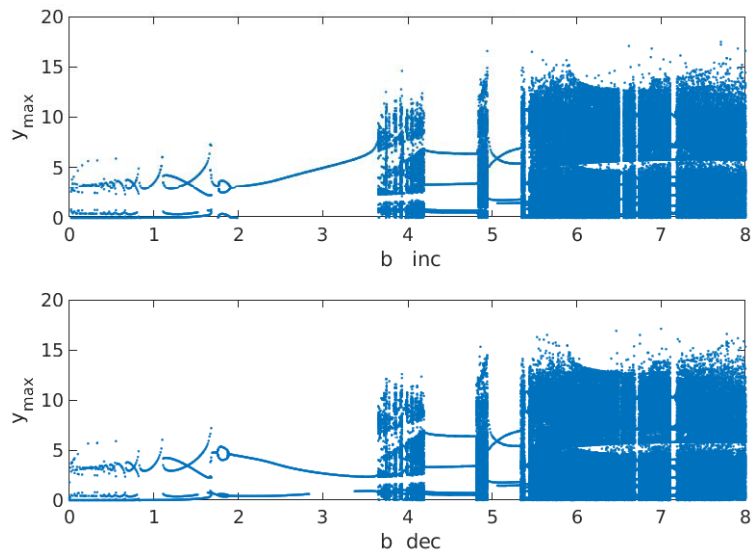

Figure 5: Bifurcation transition plots of y_{max} as b varies between $0 < b < 8$. The upper panel is for b increasing, while the lower panel is for b decreasing.

Figure 6 shows the transition plots as c varies, firstly for $0 < c < 9$, and then an enlargement of the region between $0 < c < 4$ is shown in Figure 7. This second set of plots clearly shows hysteresis.

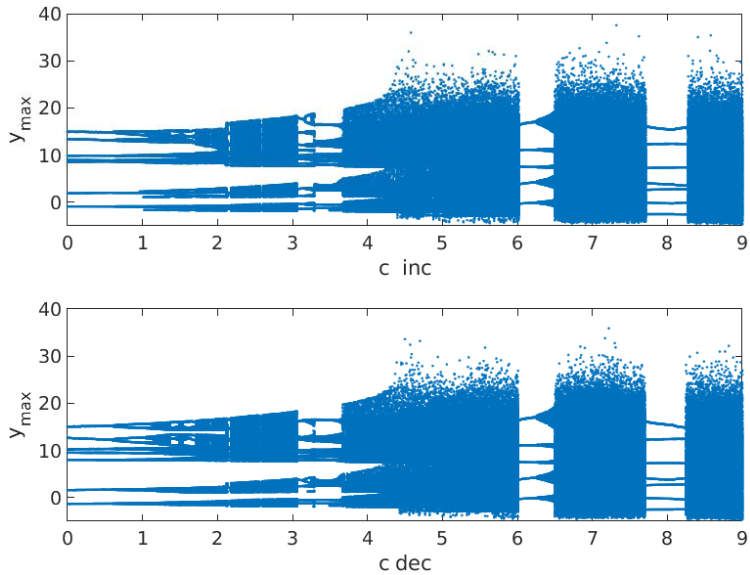

Figure 6: Bifurcation transition plots of $y_{\max}$ as c varies between $0 < c < 9$. The upper panel is for c increasing, while the lower panel is for c decreasing.

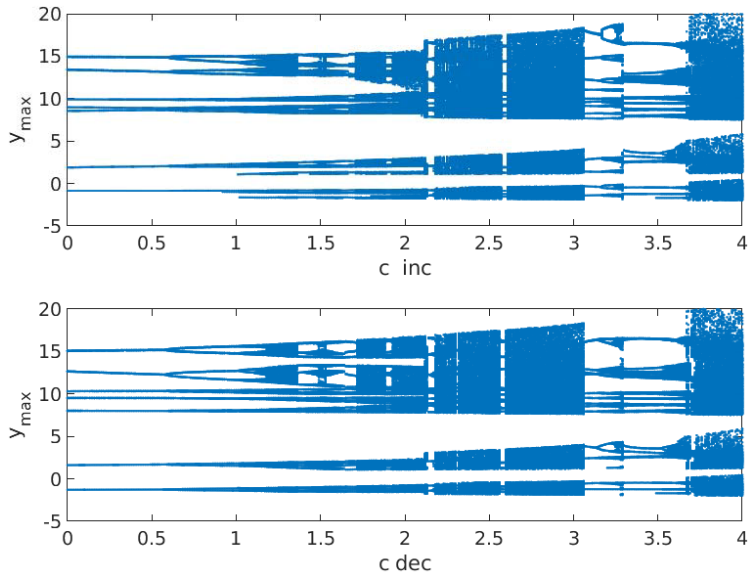

Figure 7: Bifurcation transition plots of $y_{\max}$ as c varies between $0 < c < 4$. The upper panel is for c increasing, while the lower panel is for c decreasing.

Finally, Figure 8 shows the bifurcation transition plots as d varies between $0 < d < 3.5$. Note the marked differences in the plots for d increasing and decreasing, especially in the neighbourhood of the origin.

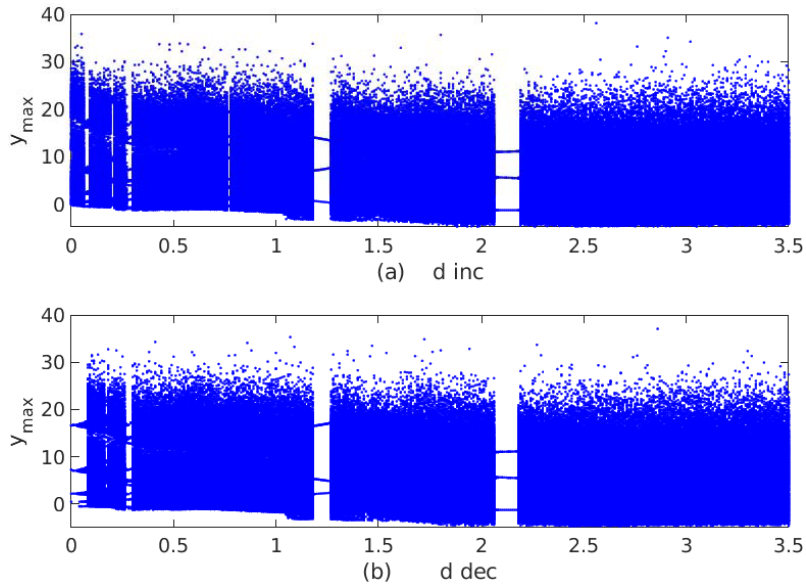

Figure 8: Bifurcation transition plots of $y_{\max}$ as d varies between $0 < d < 3.5$. The upper panel is for d increasing, while the lower panel is for d decreasing.

2.3. Period-doubling bubbles

Figure 7 shows evidence of a period-doubling bubble (forward and reverse period-doubling cascades) for $c \approx 1.5$. However there are multiple branches which undergo these bubble-bifurcations simultaneously (when $c = 0$, there are 7 branches of solutions on the $y_{\max}$ axis), which leads to a complicated scenario. Figure 9 shows four snapshots of the period-doubling bubbles as the parameter c decreases, but for different values of a. Figure 9(a) for $a = 46$ shows the beginnings of the period-doubling bubbles. There are five different branches which overlap both before and during the formation of the bubbles. In Figure 9(b) for $a = 45$, the bubbles are shown clearly. Each bubble shows a period-four cycle, but there are five bubbles, and so the repetition is every twenty. In Figure 9(c) ($a = 40$) further period-doubling cascades have occurred, but the branches are starting to cross-over again. When $a = 35$, we can see period-doubling and halving bubbles, but the halving sections are curtailed because of the expanding regions of chaotic dynamics for $c > 5.5$.

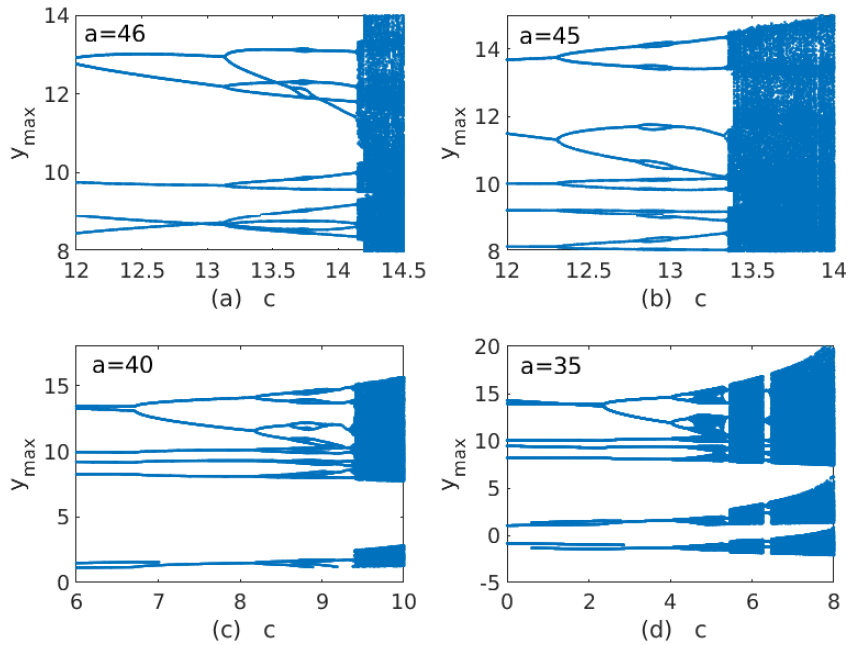

Figure 9: Four examples of period-doubling bubbles for (a) $a = 46$, (b) $a = 45$, (c) $a = 40$, (d) $a = 35$.

2.4. Multistability and coexisting attractors

Multistability means the coexistence of two or more attractors under different initial conditions but with the same parameter set. It is an interesting phenomenon and can usually be found in many nonlinear dynamical systems. It is known that multistability can lead to very complex behaviors in a dynamical system.

It is interesting that the new hyperchaotic system (1) can exhibit coexisting attractors when choosing different initial conditions. We take parameter values as in the hyperchaotic case, *viz.* $(a, b, c, d) = (31, 25, 15, 3.3)$. We select three initial conditions as $X_0 = (0.2, 0.1, 0.2, 0.1)$, $Y_0 = (-0.2, 0.1, -0.2, 0.1)$ and $Z_0 = (-0.2, -0.1, -0.2, -0.1)$, and the corresponding state orbits of the system (1) are plotted in colors blue, red and green, respectively. From Figure 10, it can be observed that the new hyperchaotic system (1) exhibits multistability with three coexisting hyperchaotic attractors.

2.5. Offset boosting of the hyperchaotic attractor

Next, we consider the possibility of offset boosting by replacing the variable z by $z + k$ in the 4-D hyperchaotic system (1), where k is a constant. This has implications for amplitude control of the underlying attractor.

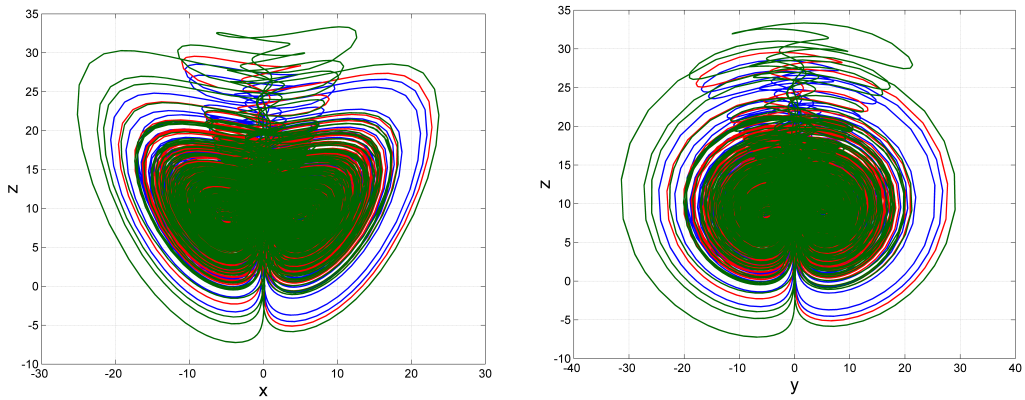

(a) (x, z)-plane (b) (y, z)-plane

Figure 10: Multi-stability of the hyperchaotic system (1): Coexisting hyperchaotic attractors for $(a, b, c, d) = (31, 25, 15, 3.3)$ and initial conditions $X_0 = (0.2, 0.1, 0.2, 0.1)$ (blue), $Y_0 = (-0.2, 0.1, -0.2, 0.1)$ (red) and $Z_0 = (-0.2, -0.1, -0.2, -0.1)$ (green).

After the transformation $z \mapsto z + k$, the system (1) can be rewritten as follows:

$$\begin{cases} \dot{x} = a(y - x), \\ \dot{y} = 2x(1 - z - k) + cy + w, \\ \dot{z} = xy - b, \\ \dot{w} = -d(x + y). \end{cases} \tag{6}$$

Figure 11 shows the results plotted in the (x, z)-plane for the choices of $k = 0$ (blue), $k = 10$ (red) and $k = 10$ (green) for the parameter choice $(a, b, c, d) =$

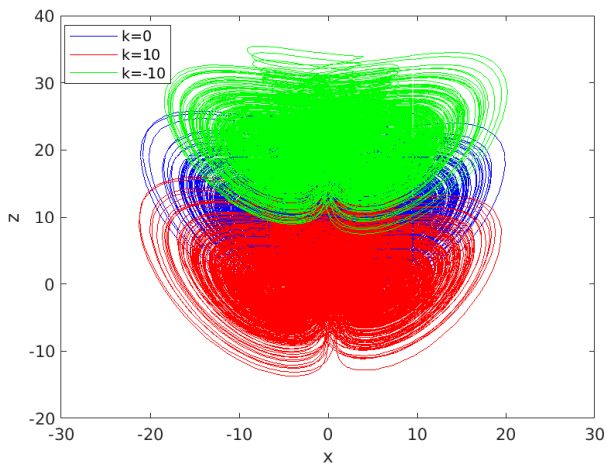

Figure 11: Three examples of offset boosting in the (x, z)-plane for the variable z for $k = 0$ (blue), $k = 10$ (red) and $k = -10$ (green).

(31, 25, 15, 3.3) which produces the hyperchaotic attractor. Varying the parameter k shifts the attractor up and down the z-axis for the new system (6).

3. Hyperchaos synchronization of the new hyperchaotic dynamical systems

As a control section, this section details the control design of achieving global hyperchaos synchronization of the new 4-D hyperchaotic dynamical system with itself (drive-response systems) via Integral Sliding Mode Control (ISMC).

As the drive system of the synchronization process, we adopt the new hyperchaotic plant

$$\begin{cases} \dot{x}_1 = a(y_1 - x_1), \\ \dot{y}_1 = 2x_1(1 - z_1) + cy_1 + w_1, \\ \dot{z}_1 = x_1 y_1 - b, \\ \dot{w}_1 = -d(x_1 + y_1), \end{cases} \tag{7}$$

where $X_1 = (x_1, y_1, z_1, w_1)$ is the state and a, b, c, d are constant parameters.

As the response system of the synchronization process, we adopt the new hyperchaotic plant

$$\begin{cases} \dot{x}_2 = a(y_2 - x_2) + v_x, \\ \dot{y}_2 = 2x_2(1 - z_2) + cy_2 + w_2 + v_y, \\ \dot{z}_2 = x_2 y_2 - b + v_z, \\ \dot{w}_2 = -d(x_2 + y_2) + v_w, \end{cases} \tag{8}$$

where $X_2 = (x_2, y_2, z_2, w_2)$ is the state and v_x, v_y, v_z, v_w are the sliding controls.

The synchronization error between the drive system (7) and the response system (8) can be defined in the following manner:

$$\begin{cases} e_x = x_2 - x_1, \\ e_y = y_2 - y_1, \\ e_z = z_2 - z_1, \\ e_w = w_2 - w_1. \end{cases} \tag{9}$$

The synchronization error dynamics is determined by a simple calculation as given below.

$$\begin{cases} \dot{e}_x = a(e_y - e_x) + v_x, \\ \dot{e}_y = 2e_x + ce_y + e_w - 2(x_2 z_2 - x_1 z_1) + v_y, \\ \dot{e}_z = x_2 y_2 - x_1 y_1 + v_z, \\ \dot{e}_w = -d(e_x + e_y) + v_w. \end{cases} \tag{10}$$

The integral sliding surface associated with each error state can be defined according to the following equations.

$$\begin{cases} \sigma_x = e_x + \lambda_x \int\limits_0^t e_x(\tau)\,\mathrm{d}\tau, \\ \sigma_y = e_y + \lambda_y \int\limits_0^t e_y(\tau)\,\mathrm{d}\tau, \\ \sigma_z = e_z + \lambda_z \int\limits_0^t e_z(\tau)\,\mathrm{d}\tau, \\ \sigma_w = e_w + \lambda_w \int\limits_0^t e_w(\tau)\,\mathrm{d}\tau. \end{cases} \tag{11}$$

Taking differentiation of each equation in (11), we derive the following:

$$\begin{cases} \dot{\sigma}_x = \dot{e}_x + \lambda_x e_x, \\ \dot{\sigma}_y = \dot{e}_y + \lambda_y e_y, \\ \dot{\sigma}_z = \dot{e}_z + \lambda_z e_z, \\ \dot{\sigma}_w = \dot{e}_w + \lambda_w e_w. \end{cases} \tag{12}$$

Using integral sliding mode control theory, we take the feedback control as follows:

$$\begin{cases} v_x = -a(e_y - e_x) - \lambda_x e_x - \tau_x \operatorname{sgn}(\sigma_x) - k_x\sigma_x, \\ v_y = -2e_x - ce_y - e_w + 2(x_2z_2 - x_1z_1) \\ \qquad -\lambda_y e_y - \tau_y \operatorname{sgn}(\sigma_y) - k_y\sigma_y, \\ v_z = -x_2y_2 + x_1y_1 - \lambda_z e_z - \tau_z \operatorname{sgn}(\sigma_z) - k_z\sigma_z, \\ v_w = d(e_x + e_y) - \lambda_w e_w - \tau_w \operatorname{sgn}(\sigma_w) - k_y\sigma_w. \end{cases} \tag{13}$$

Substitution of the control law (13) into (10) results in the closed-loop error system given below.

$$\begin{cases} \dot{e}_x = -\lambda_x e_x - \tau_x \operatorname{sgn}(\sigma_x) - k_x \sigma_x, \\ \dot{e}_y = -\lambda_y e_y - \tau_y \operatorname{sgn}(\sigma_x) - k_y \sigma_y, \\ \dot{e}_z = -\lambda_z e_z - \tau_z \operatorname{sgn}(\sigma_z) - k_z \sigma_z, \\ \dot{e}_w = -\lambda_w e_w - \tau_w \operatorname{sgn}(\sigma_w) - k_w \sigma_w. \end{cases} \tag{14}$$

We apply Lyapunov stability theory to establish the main control result of this section, which is provided in the following theorem.

Theorem 1 *The new four-dimensional hyperchaos systems (7) and (8) are globally and asymptotically synchronized for all initial states by the integral SMC law (13) where λ_x, λ_y, λ_z, λ_w, k_x, k_y, k_z, k_w, τ_x, τ_y, τ_z, τ_w are taken as positive constants.*

Proof. We consider the quadratic Lyapunov function defined by

$$V(\sigma_x, \sigma_y, \sigma_z, \sigma_w) = \frac{1}{2}\left(\sigma_x^2 + \sigma_y^2 + \sigma_z^2 + \sigma_w^2\right). \tag{15}$$

It is quite evident to observe that V is a positive definite function defined on $\mathbf{R}^4$.

The time-derivative of the function V along the error trajectories is calculated using (12) and (14) as follows:

$$\dot{V} = -\tau_x|\sigma_x| - \tau_y|\sigma_y| - \tau_z|\sigma_z| - \tau_w|\sigma_w| - k_x\sigma_x^2 - k_y\sigma_y^2 - k_z\sigma_z^2 - k_w\sigma_w^2. \tag{16}$$

Thus, $\dot{V}$ is a negative definite function defined on $\mathbf{R}^4$.

Hence, by Lyapunov stability theory, it follows that

$$(\sigma_x(t), \sigma_y(t), \sigma_z(t), \sigma_w(t)) \to 0 \quad \text{as} \quad t \to \infty$$

for all initial conditions. As a consequence, we conclude that

$$(e_x(t), e_y(t), e_z(t), e_w(t)) \to 0 \quad \text{as} \quad t \to \infty$$

for all initial conditions.

This completes the proof. □

For numerical simulations in MATLAB, we consider the parameters as in the hyperchaos case (2), *viz.* $a = 31$, $b = 25$, $c = 15$ and $d = 3.3$.

The sliding constants are chosen as follows:

We take $k_x = k_y = k_z = k_w = 10$.

We also take $\tau_x = \tau_y = \tau_z = \tau_w = 0.1$

Furthermore, we take $\lambda_x = \lambda_y = \lambda_z = \lambda_w = 10$.

The initial conditions of the drive system (7) are taken as $x_1(0) = 4.3$, $y_1(0) = 5.4$, $z_1(0) = 6.5$ and $w_1(0) = 3.1$.

The initial conditions of the response system (8) are taken as $x_2(0) = 9.6$, $y_2(0) = 1.2$, $z_2(0) = 3.8$ and $w_2(0) = 5.7$.

Figures 12–16 illustrate the sliding controller based global hyperchaos synchronization between the new hyperchaos systems (7) and (8).

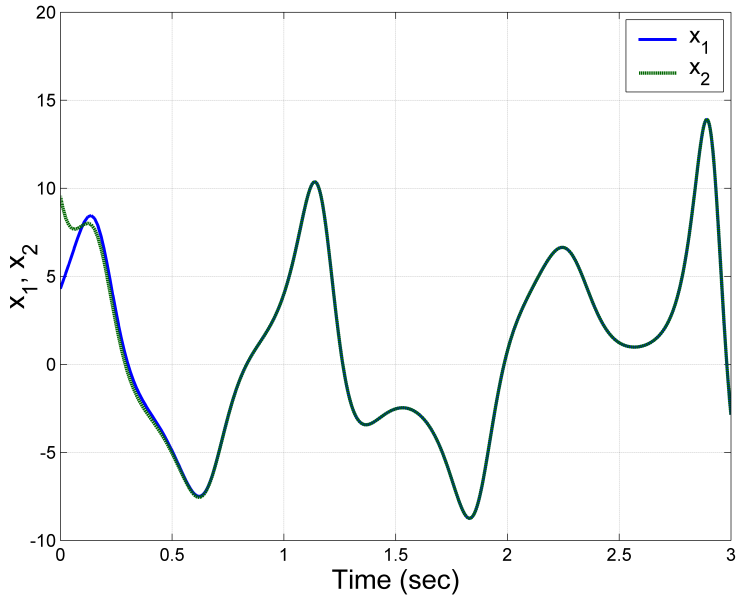

Figure 12: MATLAB simulation showing the synchronization between the states x_1 and x_2 of the new hyperchaos systems (7) and (8).

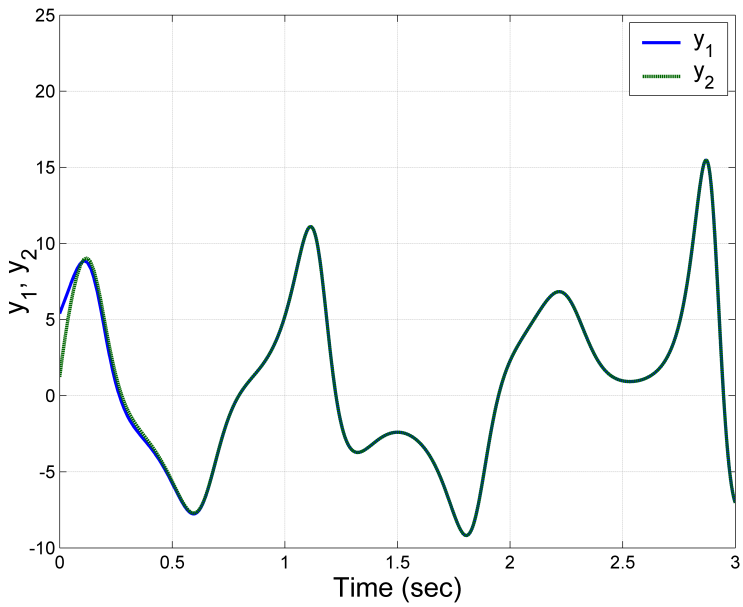

Figure 13: MATLAB simulation showing the synchronization between the states y_1 and y_2 of the new hyperchaos systems (7) and (8).

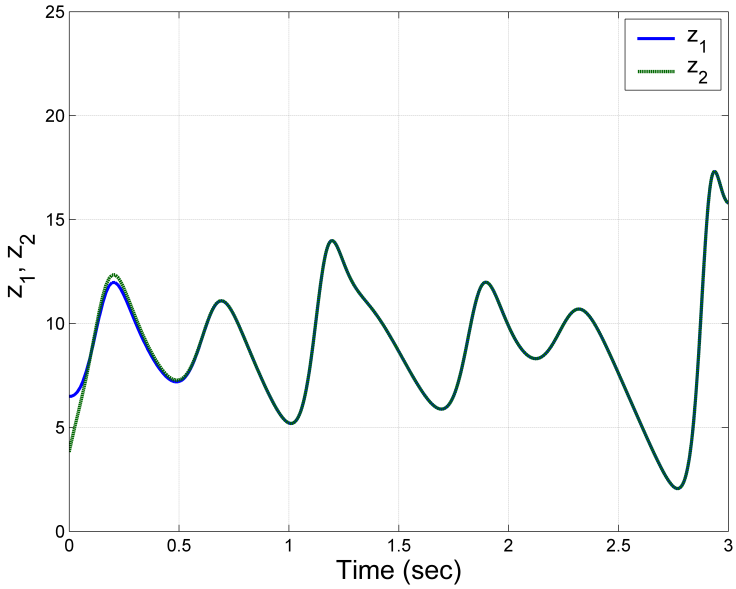

Figure 14: MATLAB simulation showing the synchronization between the states z_1 and z_2 of the new hyperchaos systems (7) and (8).

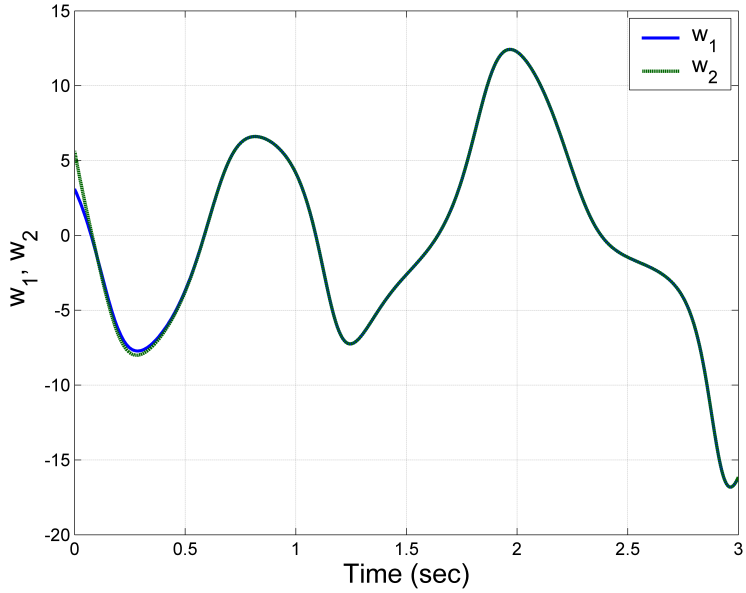

Figure 15: MATLAB simulation showing the synchronization between the states w_1 and w_2 of the new hyperchaos systems (7) and (8).

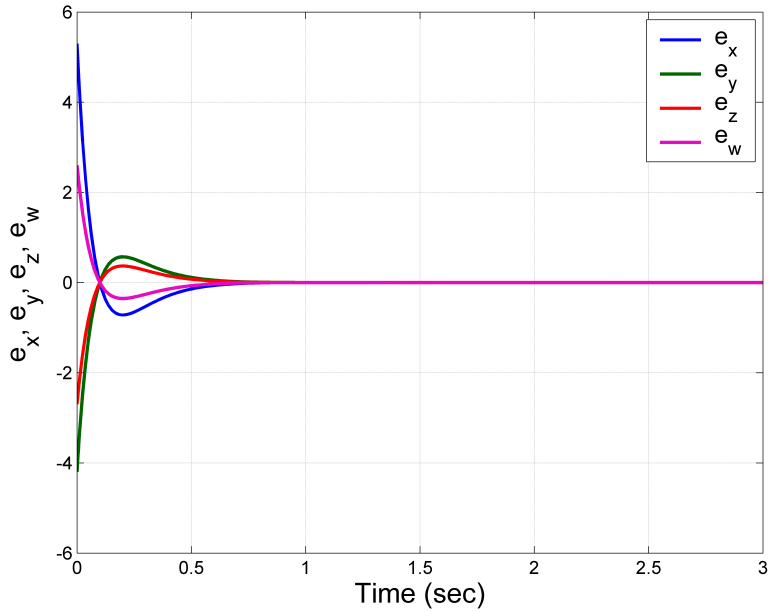

Figure 16: MATLAB simulation showing the time-history of the synchronization errors e_x, e_y, e_z, e_w between new hyperchaos systems (7) and (8).

4. An electronic circuit implementation of the new hyperchaotic system

In this section, the theoretical model of the new hyperchaotic system (1) is implemented using electronic circuits. This is realized with the Kirchhoff's circuit laws approach and Op Amp analysis. The electronic circuit diagram for system (1) is depicted in Figure 17. In this section, we set $X = \frac{1}{4}x$, $Y = \frac{1}{4}y$, $Z = \frac{1}{2}z$ and $W = \frac{1}{4}w$. After the linear scaling, we rewrite the hyperchaotic system dynamics (1) as

$$\begin{cases} \dot{X} = a(Y - X), \\ \dot{Y} = 2X - 4XZ + cY + W, \\ \dot{Z} = 8XY - \frac{b}{2}, \\ \dot{W} = -dX - dY. \end{cases} \tag{17}$$

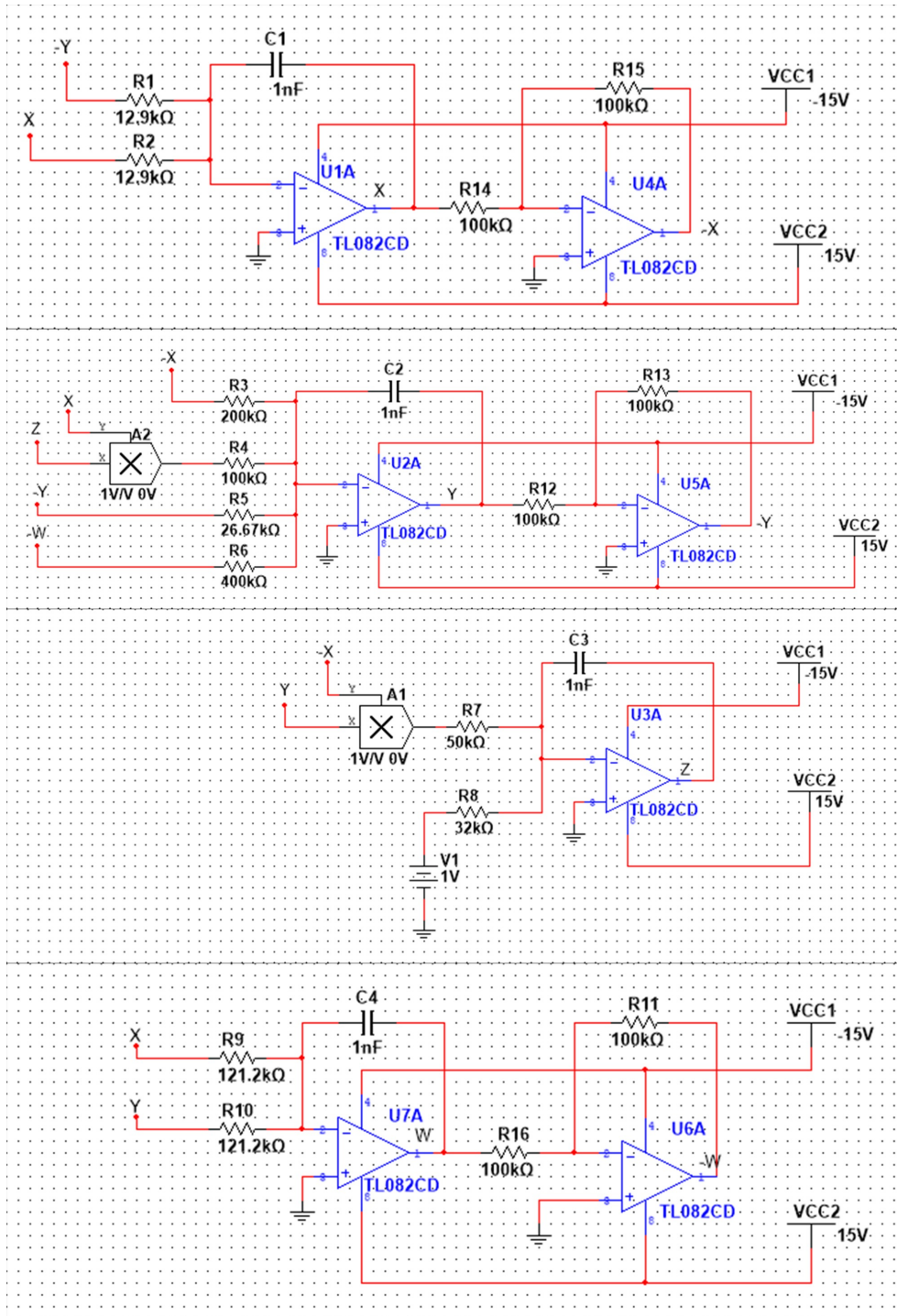

Figure 17: Dynamics of the Lyapunov exponents of the 3-D chaotic system

By applying Kirchhoff's circuit laws, we get its circuital equations as follows:

$$\begin{cases} \dot{X} = \dfrac{1}{C_1 R_1} Y - \dfrac{1}{C_1 R_2} X, \\ \dot{Y} = \dfrac{1}{C_2 R_3} X - \dfrac{1}{C_2 R_4} XZ + \dfrac{1}{C_2 R_5} Y + \dfrac{1}{C_2 R_6} W, \\ \dot{Z} = \dfrac{1}{C_3 R_7} XY - \dfrac{1}{C_3 R_8} V_1, \\ \dot{Z} = -\dfrac{1}{C_4 R_9} X - \dfrac{1}{C_4 R_{10}} Y. \end{cases} \tag{18}$$

The values of the circuit components have been chosen as: $R_1 = R_2 = 12.9\,\text{k}\Omega$, $R_3 = 200\ \text{k}\Omega$, $R_5 = 26.67\ \text{k}\Omega$, $R_6 = 400\ \text{k}\Omega$, $R_7 = 50\ \text{k}\Omega$, $R_8 = 32\ \text{k}\Omega$, $R_9 = R_{10} = 121.2\ \text{k}\Omega$, $R_4 = R_{11} = R_{12} = R_{13} = R_{14} = R_{15} = R_{16} = 100\ \text{k}\Omega$, $V_1 = 1$ volt and $C_1 = C_2 = C_3 = C_4 = 1$ nF.

The phase portraits of the circuit are represented in Figure 18. A very good similarity between MATLAB simulation results (shown in Figure 1) and Multi-Sim version 13.0 simulation results (shown in Figure 18) can be observed.

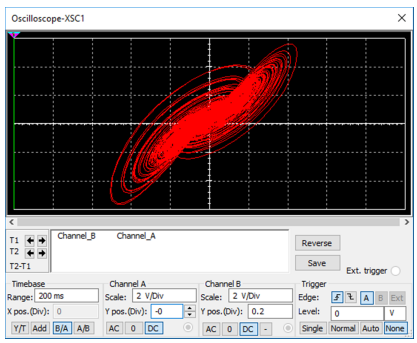

(a) (X, Y)-plane

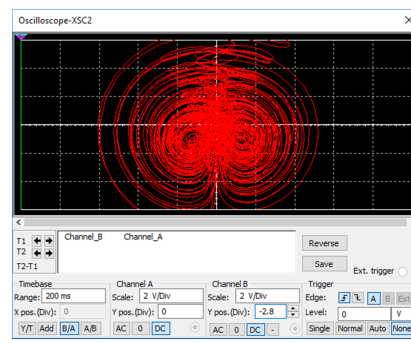

(b) (Y, Z)-plane

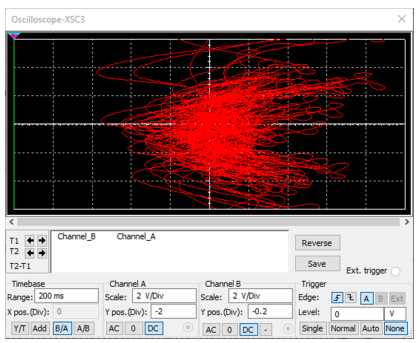

(c) (Z, W)-plane

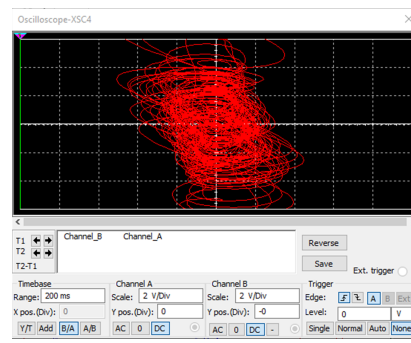

(d) (X, W)-plane

Figure 18: The phase portraits of the new hyperchaotic system in MultiSim version 13.0

5. Conclusions

We reported a new 4-D hyperchaotic dynamical system with no equilibrium in this work. This special chaotic system belongs to the class of dynamical systems with hidden attractors. We carried out a detailed qualitative analysis of the new hyperchaotic system with bifurcation transition diagrams, multistability analysis, period-doubling bubbles and offset boosting analysis. As a control application, we got new results for the global hyperchaos synchronization of the new 4-D systems using integral sliding mode control. Furthermore, an electronic circuit realization of the new hyperchaotic system was simulated in MultiSim software version 13.0 to verify the practical feasibility of the new system.

References

[1] V.T. Pham, S. Vaidyanathan, C. Volos and T. Kapitaniak: *Nonlinear Dynamical Systems with Self-Excited and Hidden Attractors*, Berlin, Springer, 2018.

[2] J.C. Antoranz and M.A. Rubio: Hyperchaos in a simple model for a laser with a saturable absorber, *Journal of the Optical Society of America B: Optical Physics*, **5**(5) (1988), 1070–1073.

[3] E.M. Shahverdiev and K.A. Shore: Time-delay hyperchaos synchronisation and implications for laser diodes subject to optical feedback, *IEE Proceedings: Optoelectronics*, **148**(1) (2001), 46–48.

[4] A.Y. Shvets and T.S. Krasnopolskaya: Hyperchaos in piezoceramic systems with limited power supply, *Solid Mechanics and its Applications*, **6** (2008), 313–322.

[5] X.Q. Feng and K. Shen: Controlling hyperchaos in a system of degenerate optical parametric oscillators by means of resonant three-wave interaction, *Technical Physics Letters*, **33**(7) (2007), 578–580.

[6] L. Borkowski: Dynamice of three unidirectionally coupled duffing oscillators, *Mechanics and Mechanical Engineering*, **15**(2) (2011), 125–132.

[7] J.S.A. Eyebe Fouda and S.L. Sabat: A multiplierless hyperchaotic system using coupled Duffing oscillators, *Communications in Nonlinear Science and Numerical Simulation*, **20**(1) (2015), 24–31.

[8] E.V. Blokhina and A.G. Rozhnev: Chaos and hyperchaos in a gyrotron, *Radiophysics and Quantum Electronics*, **49**(10) (2006), 799–810.

[9] A. Gokyildirim, Y. Uyaroglu and I. Pehlivan: A weak signal detection application based on hyperchaotic Lorenz system, *Tehnicki Vjesnik*, **25**(3) (2018), 701–708.

[10] K. Rajagopal, A. Karthikeyan and P. Duraisamy: Difference equations of a memristor higher order hyperchaotic oscillator, *African Journal of Science, Technology, Innovation and Development*, **10**(3) (2018), 279–285.

[11] F.J. Chen and J.B. Li: Hyperchaos in RTD-based cellular neural networks, *International Journal of Bifurcation and Chaos*, **8**(11) (2008), 3439–3446.

[12] Y. Huang and X.S. Yang: Hyperchaos in a new family of simple CNNs, *International Journal of Bifurcation and Chaos*, **16**(11) (2006), 3341–3348.

[13] S. Vaidyanathan: Hybrid chaos synchronization of 3-cells cellular neural network attractors via adaptive control method, *International Journal of PharmTech Research*, **8**(8) (2015), 61–73.

[14] F. Paratesh, K. Rajagopal, A. Karthikeyan, A. Alsaedi, T. Hayat and V.T. Pham: Complex dynamics of a neuron model with discontinuous magnetic induction and exposed to external radiation, *Cognitive Neurodynamics*, **12** (6) (2018), 607–614.

[15] P. Rakheja, R. Vig and P. Singh: An asymmetric hybrid cryptosystem using hyperchaotic system and random decomposition in hybrid multi resolution wavelet domain, *Multimedia Tools and Applications*, **78** (15) (2019), 20809-20834.

[16] S. Hammami: Multi-switching combination synchronization of discrete-time hyperchaotic systems for encrypted audio communication, *IMA Journal of Mathematical Control and Information*, **36**(2) (2019), 583–602.

[17] P. Rakheja, R. Vig, P. Singh and R. Kumar: An iris biometric protection scheme using 4D hyperchaotic system and modified equal modulus decomposition in hybrid multi resolution wavelet domain, *Optical and Quantum Electronics*, **51**(6) (2019), Article ID 204.

[18] J. Liu, X. Tong, Y. Liu, M. Zhang and J. Ma: A joint encryption and error correction scheme based on chaos and LDPC, *Nonlinear Dynamics*, **93**(3) (2018), 1149–1163.

[19] S. Vaidyanathan: Adaptive control of the FitzHugh-Nagumo chaotic neuron model, *International Journal of PharmTech Research*, **8**(6) (2015), 117–127.

[20] S. Wang, S. He, K. Rajagopal, A. Karthikeyan and K. Sun: Route to hyperchaos and chimera states in a network of modified Hindmarsh-Rose neuron model with electromagnetic flux and external excitation, *European Physical Journal: Special Topics*, **229** (2020), 929–942.

[21] S. Vaidyanathan, A.T. Azar, A. Akgul, C.H. Lien, S. Kacar and U. Cavusoglu: A memristor-based system with hidden hyperchaotic attractors, its circuit design, synchronisation via integral sliding mode control and an application to voice encryption, *International Journal of Automation and Control*, **13**(6), (2019) 644–647.

[22] X. Xia, Y. Zeng and Z. Li: Coexisting multiscroll hyperchaotic attractors generated from a novel memristive jerk system, *Pramana*, **91**(6) (2018), Article ID 82.

[23] P.D. Kamdem Kuate, Q. Lai and H. Fotsin: Complex behaviors in a new 4D memristive hyperchaotic system without equilibrium and its microcontroller-based implementation, *European Physical Journal: Special Topics*, **228**(10) (2019), 2171–2184.

[24] N.V. Kuznetsov and T. Mokaev: Numerical analysis of dynamical systems: Unstable periodic orbits, hidden transient chaotic sets, hidden attractors, and finite-time Lyapunov dimension, *Journal of Physics: Conference Series*, **1205**(1) (2019), Article ID 012034.

[25] S. Vaidyanathan, L.G. Dolvis, K. Jacques, C.H. Lien and A. Sambas: A new five-dimensional four-wing hyperchaotic system with hidden attractor, its electronic circuit realisation and synchronisation via integral sliding mode control, *International Journal of Modelling, Identification and Control*, **32**(1) (2019), 30–45.

[26] A. Sambas, M. Mamat, S. Vaidyanathan, M.A. Mohamed, W.S. Mada Sanjaya and Mujiarto: A novel chaotic hidden attractor, its synchronization and circuit implementation, *WSEAS Transactions on Systems and Control*, **13** (2018), 345–352.

[27] S. Vaidyanathan, A.T. Azar and A. Boulkroune: A novel 4-D hyperchaotic system with two quadratic nonlinearities and its adaptive synchronisation, *International Journal of Automation and Control*, **12**(1) (2018), 5–26.

[28] S. Vaidyanathan: Adaptive integral sliding mode controller design for the regulation and synchronization of a novel hyperchaotic finance system with a stable equilibrium, *Studies in Computational Intelligence*, **709** (2017), 289–318.

[29] N.V. Kuznetsov, T.N. Mokaev, E.V. Kudryashova, O.A. Kuznetsova, R.N. Mokaev, M.V. Yuldashev and R.V. Yuldashev: Stability and chaotic attractors of memristor-based circuit with a line of equilibria, *Lecture Notes in Electrical Engineering*, **554** (2020), 639–644.

[30] S. Fang, Z. Li, X. Zhang and Y. Li: Hidden extreme multistability in a novel no-equilibrium fractional-order chaotic system and its synchronization control, *Brazilian Journal of Physics*, **49**(6) (2019), 846–858.

[31] X. Li and Z. Li: Hidden extreme multistability generated from a fractional-order chaotic system, *Indian Journal of Physics*, **93**(12) (2019), 1601–1610.

[32] E.F. Doungmo Goufo: On chaotic models with hidden attractors in fractional calculus above power law, *Chaos, Solitons and Fractals*, **127** (2019), 24–30.

[33] X. Zhang and Z. Li: Hidden extreme multistability in a novel 4D fractional-order chaotic system, *International Journal of Non-Linear Mechanics*, **111** (2019), 14–27.

[34] A. Bayani, K. Rajagopal, A.J.M. Khalaf, S. Jafari, G.D. Leutchi and J. Kengne: Dynamical analysis of a new multistable chaotic system with hidden attractor: Antimonotonicity, coexisting multiple attractors, and offset boosting, *Physics Letters, Section A: General, Atomic and Solid State Physics*, **383**(13) (2019), 1450–1456.

[35] C.Y. Chen, K. Rajagopal, I.I. Hamarash, F. Nazarimehr, F.E. Alsaadi and T. Hayat: Antimonotonicity and multistability in a fractional order memristive chaotic oscillator, *European Physical Journal: Special Topics*, **228**(10) (2019), 1969–1981.

[36] Y. Zhang, Z. Liu, H. Wu, S. Chen and B. Bao: Two-memristor-based chaotic system and its extreme multistability reconstitution via dimensionality reduction analysis, *Chaos, Solitons and Fractals*, **127** (2019), 354–363.

[37] I. Ahmad, B. Srisuchinwong and W. San-Um: On the first hyperchaotic hyperjerk system with no equilibria: A simple circuit for hidden attractors, *IEEE Access*, **6** (2018), 35449–35456.

[38] M. Wang, X. Liao, Y. Deng, Z. Li, Y. Su and Y. Zeng: Dynamics, synchronization and circuit implementation of a simple fractional-order chaotic system with hidden attractors, *Chaos, Solitons and Fractals*, **130** (2020), Article ID 109406.

[39] S. Vaidyanathan: Output regulation of Arneodo-Coullet chaotic system, *Communications in Computer and Information Science*, **133** (2011), 98–107.

[40] S. Vaidyanathan: Output regulation of the unified chaotic system, *Communications in Computer and Information Science*, **198** (2011), 1–9.

[41] S. Vaidyanathan: Adaptive control and synchronization design for the Lu-Xiao chaotic system, *Lecture Notes in Electrical Engineering*, **131** (2013), 319–327.

[42] S. Vaidyanathan: Global chaos synchronization of the forced Van der Pol chaotic oscillators via adaptive control method, *International Journal of PharmTech Research*, **8**(6) (2015), 156–166.

[43] S. Vaidyanathan: Chaos in neurons and adaptive control of Birkhoff-Shaw strange chaotic attractor, *International Journal of PharmTech Research*, **8**(5), (2015), 956–963.

[44] Y. Li, B. Yang, X. Zhang, Q. Wu and T. Zheng: Extended state observer-based intelligent double integral sliding mode control of electronic throttle valve, *Advances in Mechanical Engineering*, **9**(12) (2017), 1–10.

[45] A. Chibani, B. Daaou, A. Gouichiche, A. Safia and Y. Messlem: Finite-time integral sliding mode control for chaotic permanent magnet synchronous motor systems, *Archives of Electrical Engineering*, **66**(2) (2017), 229–239.

[46] N.V. Stankevich, O.V. Astakhov, A.P. Kuznetsov and E.P. Seleznev: Exciting chaotic and quasi-periodic oscillations in a multicircuit oscillator with a common control scheme, *Technical Physics Letters*, **44**(5) (2018), 428–431.

[47] S. Vaidyanathan, M. Feki, A. Sambas and C.H. Lien: A new biological snap oscillator: Its modelling, analysis, simulations and circuit design, *International Journal of Simulation and Process Modelling*, **13**(5) (2018), 419–432.

[48] V.T. Pham, S. Jafari, S. Vaidyanathan, C. Volos and X. Wang: A novel memristive neural network with hidden attractors and its circuitry implementation, *Science China Technological Sciences*, **59**(3) (2016), 358–363.

[49] W. Zhou, G. Wang, H.H.C. Lu, Y. Shen and Y. Liang: Complex dynamics of a non-volatile memcapacitor-aided hyperchaotic oscillator, *Nonlinear Dynamics*, **100**(4) (2020), 3937–3957.

[50] A. Wolf, J.B. Swift, H.L. Swinney and J.A. Vastano: Determining Lyapunov exponents from a time series, *Physica D*, **16** (1985), 285–317.